NeuroImage: Clinical 18 (2018) 382–389

Contents lists available at ScienceDirect

NeuroImage: Clinical

journal homepage: www.elsevier.com/locate/ynicl

Deficits of entropy modulation in schizophrenia are predicted by functional connectivity strength in the theta band and structural clustering

Javier Gomez-Pilar[a,1], Rodrigo de Luis-García[b,1], Alba Lubeiro[c], Nieves de Uribe[d], Jesús Poza[a,e,f], Pablo Núñez[a], Marta Ayuso[g], Roberto Hornero[a,e,f], Vicente Molina[c,d,e,*]

[a] Biomedical Engineering Group, University of Valladolid, Paseo de Belén, 15, 47011 Valladolid, Spain
[b] Imaging Processing Laboratory, University of Valladolid, Paseo de Belén, 15, 47011 Valladolid, Spain
[c] Psychiatry Department, School of Medicine, University of Valladolid, Av. Ramón y Cajal, 7, 47005 Valladolid, Spain
[d] Psychiatry Service, Clinical Hospital of Valladolid, Ramón y Cajal, 3, 47003 Valladolid, Spain.
[e] Neurosciences Institute of Castilla y León (INCYL), Pintor Fernando Gallego, 1, 37007, University of Salamanca, Spain
[f] IMUVA, Mathematics Research Institute, University of Valladolid, Valladolid, Spain
[g] Neurophysiology Service, Clinical Hospital of Valladolid, Ramón y Cajal, 3, 47003 Valladolid, Spain

ARTICLE INFO

Keywords:
Schizophrenia
Entropy
Graph-theory
Connectivity
Fractional anisotropy
Negative symptoms

ABSTRACT

Spectral entropy (SE) allows comparing task-related modulation of electroencephalogram (EEG) between patients and controls, i.e. spectral changes of the EEG associated to task performance. A SE modulation deficit has been replicated in different schizophrenia samples. To investigate the underpinnings of SE modulation deficits in schizophrenia, we applied graph-theory to EEG recordings during a P300 task and fractional anisotropy (FA) data from diffusion tensor imaging in 48 patients (23 first episodes) and 87 healthy controls. Functional connectivity was assessed from phase-locking values among sensors in the theta band, and structural connectivity was based on FA values for the tracts connecting pairs of regions. From those data, averaged clustering coefficient (CLC), characteristic path-length (PL) and connectivity strength (CS, also known as density) were calculated for both functional and structural networks. The corresponding functional modulation values were calculated as the difference in SE and CLC, PL and CS between the pre-stimulus and response windows during the task. The results revealed a higher functional CS in the pre-stimulus window in patients, predictive of smaller modulation of SE in this group. The amount of increase in theta CS from pre-stimulus to response related to SE modulation in patients and controls. Structural CLC was associated with SE modulation in the patients. SE modulation was predictive of negative symptoms, whereas CLC and PL modulation was associated with cognitive performance in the patients. These results support that a hyperactive functional connectivity and/or structural connective deficits in the patients hamper the dynamical modulation of connectivity underlying cognition.

1. Introduction

Mental functions are partially based on the dynamic coordination of cerebral networks (Dehaene and Changeux, 2011; Tanaka, 1996; Varela et al., 2001) whose interactions evolve in hundreds of milliseconds (Bressler and Tognoli, 2006; Sporns, 2011). The temporal resolution of electroencephalography (EEG) allows the assessment of this dynamic coordination, which can be applied to the study of functional underpinnings of mental disorders. Measurements summarizing the EEG properties and their modulation with cognition can be useful for that purpose. One of these measurements is Spectral Entropy (SE), a parameter derived from information theory that estimates regularity by quantifying the degree of uncertainty in a signal (Duff et al., 2013). Larger SE values correspond to more uniform spectra whose frequency content is broader (i.e., more random), and low SE values to spectra with only a few frequency components (i.e., more regular).

In schizophrenia, we have described a SE modulation deficit during a P300 task in response to relevant tones (Bachiller et al., 2014). SE decreased in healthy controls secondarily to task-related increased theta power, and both SE decrease and theta power increase were of smaller magnitude in patients (Bachiller et al., 2014), which seems coherent with the expected increase in theta band power during P300 (Mazaheri and Picton, 2005). Later, we replicated the same SE modulation deficit in schizophrenia in a larger and completely different

* Corresponding author.
E-mail address: vicente.molina@uva.es (V. Molina).
[1] Javier Gomez-Pilar and Rodrigo de Luis are co-first authors.

https://doi.org/10.1016/j.nicl.2018.02.005
Received 18 November 2017; Received in revised form 10 January 2018; Accepted 4 February 2018
Available online 06 February 2018

sample (Molina et al., 2017a), showing its relation to cognition and symptoms. In these reports we defined modulation as the difference in SE values between the pre-stimulus and the response windows of the P300 task being performed by the subjects. Neither treatment dose nor illness duration were associated to the SE deficit, also found in first episode patients.

Given the apparent robustness of the SE modulation deficit, we considered it worthy to attempt to characterize it. This could help describing a reliable functional alteration in schizophrenia. Since cognition during P300 involves a global network rather than focal engagement (Bledowski et al., 2004), we hypothesized that the analysis of global properties of the functional network would help to identify underpinnings of the SE modulation deficit in schizophrenia. Global network properties can be assessed at system level using graph theory. Thus, parameters derived from graph-theory can help assessing both basal network properties predictive of SE modulation and properties of global network dynamics associated to SE modulation deficits.

Among the graph parameters of interest to this purpose, local clustering coefficient (*CLC)* is related to the degree of local connectivity. Specifically, clustering coefficient is the ratio between the number of triangles in which a node is included and the total number of possible triangles that include the node. This measure, when averaged across the network, indicates the segregation and local efficiency for information transfer. In turn, characteristic path length (*PL*) is the average of shortest distances for all possible pairs of nodes. Thus, *PL* is related to information integration across areas. Mean connectivity strength (*CS*, sometimes also known as density) in a weighted graph can be interpreted as the average of connections among nodes in a network. The application of these parameters to functional connectivity analyses is based on the degree of similarity of signals, based in turn on phase-locking values (PLV) of the signals between regions or (for the EEG) sensors. These parameters can be also applied to structural connectivity measurements derived from diffusion magnetic resonance imaging (dMRI), such as fractional anisotropy (FA), which may allow a description of the dependence of functional connectivity modulation on structural connectivity. Although a direct relation between both connectivity dimensions could seem intuitive, functional connections are found between regions without direct anatomical connections (Honey et al., 2009).

Our hypotheses are that functional (prior to cognitive activity) and structural graph-derived network measurements would predict task-related SE modulation and that the dynamics of functional network parameters would be associated to SE modulation. As in previous reports (Bachiller et al., 2014; Mazaheri and Picton, 2005) modulation will be defined and the corresponding EEG change (for SE and functional network parameters) associated to task performance. These ideas could reveal relevant insights on the functional deficits in schizophrenia. Based on previous findings supporting a smaller increase of theta power in patients in the response to target (Bachiller et al., 2014) and the relevance of theta power for the task used, the P300 (Mazaheri and Picton, 2005), we focused our analyses on the theta EEG band.

2. Subjects and methods

We included 48 schizophrenia subjects (of them, 23 first episodes (FE) and 87 healthy subjects with normal hearing. Patients were diagnosed according to the Diagnostic and Statistical Manual of Mental Disorders, 5th edition. They were receiving stable doses of antipsychotic monotherapy. Of them, MRI data were also collected in 33 patients (20 males) and 24 controls (15 males). Out of the sample, 42 patients and 65 controls were included in a previous report on SE modulation deficit in schizophrenia (Molina et al., 2017a).

First episode patients were treated with antipsychotics for less than 72 h. prior to MRI and EEG data acquisition, with a wash-out period of 24 h prior to the acquisitions to avoid possible bias due to the selection of patients able to cooperate during EEG acquisition without prior treatment.

Table 1
Demographic, clinical and cognitive characteristics of patients and controls, as well as latency and amplitude of the P300 (P3b) potential. Between-group statistically significant differences were marked with asterisks: $^{***}p < 0.001$.

	Controls	*Patients*
Age (years)	30.51 (10.77)	33.58 (9.27)
Antipsychotic dose (CPZ equivalents)	N/A	377.92 (196.94)
Duration (months)	N/A	97.84 (116.94)
Sex	44/43	25/23
Positive symptoms	N/A	11.63 (3.39)
Negative symptoms	N/A	18.03 (7.52)
Total PANSS score	N/A	54.35 (18.56)
Verbal memory***	51.65 (8.26)	33.92 (12.74)
Working memory***	21.46 (3.90)	15.81 (5.01)
Motor speed***	68.59 (17.84)	58.14 (14.41)
Verbal fluency***	27.13 (5.33)	17.99 (5.70)
Performance speed***	68.79 (13.25)	42.83 (15.78)
Problem solving***	17.54 (2.72)	15.40 (4.64)
Total IQ***	111.83 (11.87)	91.22 (14.19)
WCST (perseverative errors)***	10.17 (5.81)	27.31 (47.43)
WCST (completed categories)***	5.79 (0.72)	4.39 (1.87)
P3b amplitude (microvolts)***	3.20 (1.76)	1.92 (1.21)
P3b latency (miliseconds)	472.28 (67.54)	461.53 (87.57)

Exclusion criteria were: (i) any neurological illness; (ii) history of cranial trauma with loss of consciousness; (iii) past or present substance abuse, except nicotine or caffeine (iv) intelligence quotient (IQ) smaller than 70; and (iv) for patients, any other psychiatric process, and (v) for controls, any psychiatric or neurological diagnosis or treatment.

Schizophrenia symptoms were scored using the Positive and Negative Syndrome Scale (PANSS) (Kay et al., 1987). Healthy controls were recruited through advertisements. Demographic and clinical data are shown in Table 1.

Cognitive data for both groups were collected using: the Wechsler Adult Intelligence Scale, WAIS-III (IQ), the Wisconsin Card Sorting Test (WCST; completed categories and percentage of perseverative errors), and the Spanish version of the Brief Assessment in Cognition in Schizophrenia Scale (BACS)(Segarra et al., 2011).

After receiving full printed information, subjects gave their written informed consent. The ethical committees of the Hospital Clínico de Valladolid endorsed the study.

2.1. EEG processing

2.1.1. EEG acquisition and preprocessing

EEG recordings were obtained following MRI scans, after a resting period of 30 minutes. Data were recorded using a 17-channel EEG system (BrainVision®, Brain Products GmbH). Active electrodes were placed in an elastic cap at Fp1, Fp2, F3, F4, F7, F8, C3, C4, P3, P4, O1, O2, T5, T6, Fz, Pz and Cz (international 10–20 system). Impedance was kept under 5 kΩ. Sampling frequency was 500 Hz. During EEG acquisition, each channel was referenced over Cz electrode and re-referenced to the average activity of all active sensors (Bledowski et al., 2004; Gomez-Pilar et al., 2018). Thirteen minutes of eyes-closed EEG was obtained during an auditory odd-ball 3-stimulus paradigm, which consisted of 600 random sequences of target (500 Hz-tone, probability 0.2), distractor (1000 Hz-tone, probability 0.2), and standard (2000 Hz-tone, probability 0.6) tones. The tone duration was 50 ms, rise and fall time being 5 ms and intensity being 90 dB. Inter-stimulus interval between tones randomly jittered between 1.16 and 1.44 s. The participants were asked to press a button whenever they detected the target tones. Target tones were considered ‘attended tones’ when they were followed by a button press. Only ‘attended’ target tones were taken into account for further analysis (Gomez-Pilar et al., 2015). Alertness differences across groups were controlled by comparing accuracy of target responses.

A three-step artifact rejection algorithm was applied to minimize electrooculographic and electromyographic contamination (Bachiller et al., 2015a): (i) an Independent Component Analysis (ICA) was carried out to discard noisy ICA components; (ii) after ICA reconstruction, EEG signals were divided into trials of 1 s length (ranging from 300 ms before stimulus onset to 700 ms after stimulus onset); and (iii) an automatic method was applied to reject trials whose amplitude exceeded an adaptive statistical-based threshold (Nunez et al., 2017). In this last method, the mean and standard deviation of each channel and for each stimulus was computed. Then, trials that exceeded mean ± 4 × standard deviation in at least two channels were discarded. This ensures to obtain artifact-free trials for all channels.

Signals were band-pass filtered between 1 and 70 Hz. In addition, a 50 Hz notch filter was used to remove the power line artifact.

2.1.2. EEG entropy

Entropy is a thermodynamic function adapted from information theory. Entropy can be seen as a measure of the irregularity of a signal, estimating the degree of disorder by assessing the distribution of its spectral components. In this study, the continuous wavelet transform was used to compute the entropy of the signals. The spectral entropy (SE) can be defined as follows:

$$SE(k) = \frac{1}{\log(M)} \bullet \sum_{s} WS_{\mathrm{n}}(k,s) \bullet log\left[WS_{\mathrm{n}}(k,s)\right], \tag{1}$$

where WS_n is the normalized wavelet scalogram, k is the time interval, and s the scaling factor of the mother wavelet. In order to avoid edge effects in continuous wavelet transform (CWT), the cone of influence (COI) for pre-stimulus and response time windows was computed. The SE was computed in the broadband, i.e. between 1 Hz and 70 Hz, since we want to describe the overall SE dynamics.

2.1.3. EEG brain graphs

EEG brain graphs provide a useful tool to characterize the functional brain network. Using this approach, network nodes are represented by electrodes, whereas network edges are set by computing the neural coupling between pairs of electrodes. Different methods can be used to estimate the neural coupling. In this study, we selected the PLV across successive trials (Lachaux et al., 1999), since it is sensitive to both low-amplitude oscillatory EEG components (Spencer et al., 2003) and nonlinearities (van Diessen et al., 2015). PLV can be computed using different methodologies. We used the CWT to compute the phase information from each trial (Bob et al., 2008). As in the SE computation, cones of influence were also considered.

Functional connectivity matrices were constructed using PLV values to characterize the neural coupling between each pair of electrodes. With no thresholding applied, these matrices ranged between 0 and 1, thereby, functional connectivity matrices were also constrained based on PLV ranged between 0 and 1: a value of 0 is obtained when signals do not show any synchronization and a value of 1 is observed when two signals are perfectly synchronized.

2.1.3.1. Graph parameters. After using CWT approach to perform filtering and phase extraction in one operation, the PLV between two signals $x(t)$ and $y(t)$ can be obtained evaluating the variability of the phase difference across successive trials:

$$PLV_{xy}(k,s) = \frac{1}{Nt}\left|\sum_{n=1}^{N} e^{\Delta\varphi_{xy}(k,s,n)}\right|, \tag{2}$$

where N_t is the number of trials, $\Delta\varphi_{xy}$ is the instantaneous phase difference between x and y signals, k is the time interval, and s the scaling factor of the mother wavelet.

Firstly, the event-related wave was computed for each subject by the synchronized averaging of all the trials corresponding to attended target tones. Secondly, a low-pass finite impulse response filter with cut-off frequency of 8 Hz was applied to the evoked wave in order to obtain only the components related to delta and theta frequency bands. Thirdly, the maximum amplitude of the low-pass filtered evoked wave in the Pz channel was located into a window ranging from 250 to 550 ms from the stimulus onset (Bachiller et al., 2015b). The corresponding sample to the maximum amplitude was used as a central time sample of the response window. Finally, the response window was set on ± 150 ms around the central time sample.

Normalized *CLC* and *PL* can be defined as:

$$CLC = \frac{C}{C^{random}}, \tag{3}$$

$$PL = \frac{L}{L^{random}}, \tag{4}$$

where C and L can be defined as:

$$C = \frac{1}{N}\sum_{i=1}^{N} \frac{\sum_{i\neq j}\sum_{j\neq l}^{i\neq l} w_{ij}w_{il}w_{jl}}{\sum_{i\neq j}\sum_{j\neq l}^{i\neq l} w_{ij}w_{il}}, \tag{5}$$

$$L = \frac{N(N-1)}{\sum_{i=1}^{N}\sum_{j\neq i}^{N}\frac{1}{L_{ij}}}, \tag{6}$$

Finally, the connectivity strength was computed using the network density as:

$$D = \frac{\sum_{i=1}^{N}\sum_{j>i} w_{ij}}{T}. \tag{7}$$

In the previous equations, w_{ij} refers to PLV between nodes i and j (for functional analyses) or to the structural connectivity between two regions using the streamlines from MRI (for structural analyses). N is the total number of nodes of the network (17 in EEG analyses, 84 in MRI). L_{ij} is defined as the inverse of the network edge weight w_{ij} (Stam et al., 2009). Finally, in Eq. (7), $T = N(N-1)/2$, which is the total number of connections in an undirected graph.

2.1.4. Segmentation of the EEG response

The modulation of the graph parameters along the odd-ball task was assessed by considering two windows: (i) the pre-stimulus window, which is a period of expectation before the stimulus onset, ranging from -300 ms to the stimulus onset; and (ii) the response window, chosen to capture the P3b response (150 to 450 ms after stimulus onset).

2.2. MRI acquisition and processing

A Philips Achieva 3 Tesla Unit (Philips Healthcare, Best, The Netherlands) at the MRI facility from Valladolid University was employed. Acquisitions consisted of a T1-weighted (anatomical) image and diffusion weighted images. A pipeline processing was carried out in order to obtain structural connectivity matrices (structural connectomes), as described in (Molina et al., 2017b).

For the T1 images, a turbo field echo (TFE) sequence was employed, and parameters included the following: 256 × 256 matrix size, 1 × 1 × 1 mm^3 of spatial resolution and 160 slices covering the whole brain.

With regard to the diffusion weighted images (DWIs), a single shot EPI (echo planar imaging) spin echo sequence was employed. 61 gradient directions and one baseline volume were acquired, with b-value = 1000 s/mm^2, 2 × 2 × 2 mm^3 of voxel size, 128 × 128 matrix and 66 axial slices covering the entire brain.

From the acquired images, a processing pipeline was designed in order to employ both the T1-weighted and the diffusion images for the construction of structural connectivity matrices. This pipeline is composed of several steps and uses different freely available software tools (FSL, Freesurfer, MRTRIX).

The processing pipeline of the acquired MRI volumes is designed to

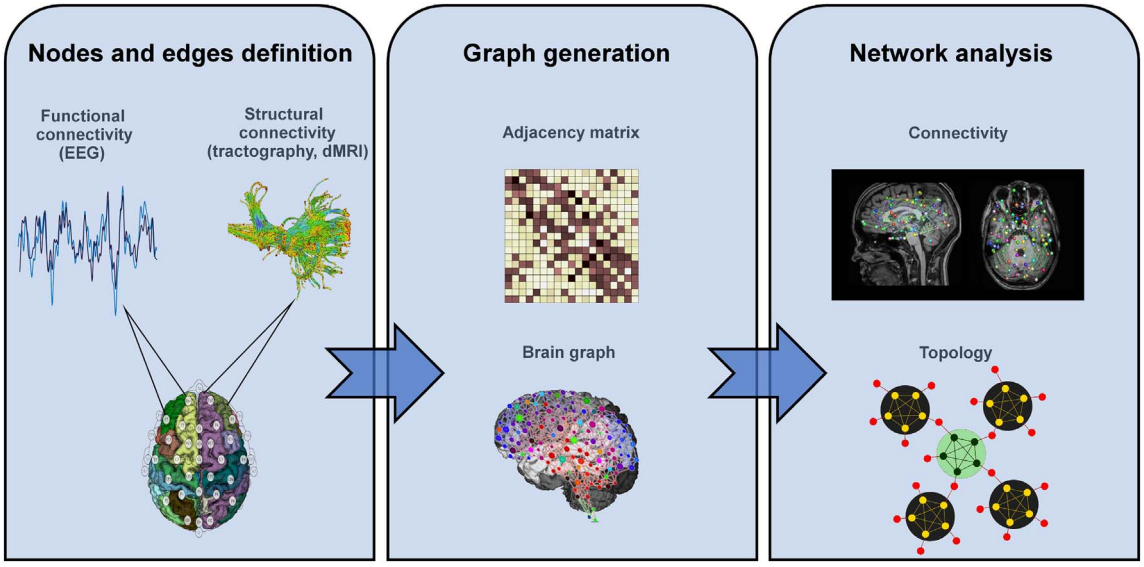

Fig. 1. Schematic overview for the network analyses from the structural and functional data.

obtain structural connectivity matrices by using both the anatomical (T1-weighted) and diffusion images.

Firstly, non-brain structures were removed from the T1 images by means of BET, a brain extraction tool from the FSL software (http://fsl.fmrib.ox.ac.uk) (Smith, 2002). Next, 84 cortical structures were segmented using Freesurfer (https://surfer.nmr.mgh.harvard.edu) (Fischl et al., 2004; Desikan et al., 2006). Also starting from the same T1 images, gray matter, white matter and cerebrospinal fluid (CSF) were also segmented, and subcortical gray matter structures were delineated using FAST and FIRST utilities from FSL, respectively (Patenaude et al., 2011; Zhang et al., 2001), and combined into a volume called 5tt (5-tissue-type) image.

At the same time, and starting from the diffusion weighted images (DWI), the brain was extracted using DWI2MASK tool from MRtrix (www.mrtrix.org) (Dhollaner and Connelly, n.d.). Afterwards, orientation distribution functions were estimated from the diffusion data using spherical deconvolution, employing DWI2RESPONSE and DWI2FOD tools from MRtrix (Tournier et al., 2007). This method allows the use of diffusion information beyond the tensor model, thus overcoming traditional problems of tensor-based tractography such as its bad behavior in fiber crossings and kissings, which are abundant in the white matter. The method of choice for fiber tracking (anatomically-constrained tractography, using TCKGEN -ACT) uses both the diffusion data and the 5tt image (after registration) in order to discard streamlines that are anatomically unfeasible. Two million streamlines were generated for each subject.

In order to describe the diffusion at each voxel, diffusion tensors were estimated using a least squares method (Salvador et al., 2005), and Fractional Anisotropy (FA) volumes were computed from the diffusion tensors using DTIFIT tool from FSL. FA quantifies the amount of anisotropy in the diffusion tensor or, equivalently, how much it deviates from a totally isotropic diffusion. FA is usually interpreted as a descriptor of white matter integrity, and decreases in FA have been related to alterations in the white matter due to several factors (demyelination and axonal destruction, among others).

Finally, connectivity matrices were constructed from the tractography results and the (registered) cortical segmentations using TCK2CONNECTOME tool from MRtrix. When streamlines (tractography output) connecting two cortical regions were found, this tool computes the average FA for that specific connection. Thus, 84 × 84 connectivity matrices were obtained using FA as connectome metrics. A threshold was not applied to the connectivity matrices; however, some matrix coefficients can be equal to zero when streamlines are not found for that particular connection.

Similar dMRI analyses have been reported in schizophrenia (Di Biase et al., 2017) and other neurocognitive conditions (Jones et al., 2015).

2.3. Graph-theory parameters

From both the structural and functional connectivity matrices, we calculated three graph-theory parameters to characterize global properties of the brain network: (i) connectivity strength by means of network density (*CS*), (ii) network segregation using *CLC*, and (iii) network integration by means of *PL* (Rubinov and Sporns, 2010). *CLC* and *PL* were computed over an ensemble of 50 surrogate random networks, which were used to normalize *CLC* and *PL* values obtained from the original networks (Stam et al., 2009). This widespread method is useful to obtain graph parameters independent of the network edge weights and the network size.

As opposed to the broadband approach used to compute de SE, functional parameters were computed into the theta frequency range during pre-stimulus and task-related modulation (i.e. difference between the response and the pre-stimulus windows) and will be referred to as $EEG\text{-}PL_{PRE}$, $EEG\text{-}CS_{PRE}$ and $EEG\text{-}CLC_{PRE}$, for the pre-stimulus parameters, and as $EEG\text{-}PL_{MOD}$, $EEG\text{-}CS_{MOD}$ and $EEG\text{-}CLC_{MOD}$, for the modulation-related parameters. On the other hand, structural parameters will be referred to as *dMRI-PL*, *dMRI-CS* and *dMRI-CLC*.

The present data do not duplicate our published EEG network analyses in schizophrenia (Gomez-Pilar et al., 2017), since those were performed in a different sample using evoked response instead of single-trial analyses.

A schematic overview for the network analyses both for functional and for structural data is shown in Fig. 1.

3. Statistics

After testing parametric test assumptions, demographic, cognitive and P300 latency and amplitude values were compared between patients and controls using Chi-square and *t* tests.

Network measurements were also compared between patients and controls using *t* tests. When significant differences were found between groups, the corresponding values were compared between chronic and FE patients.

To test the main study hypothesis, in a first step we applied a principal component analysis (PCA) with varimax rotation to individual

SE modulation values, thus reducing the number of SE modulation measurements (one per electrode) to one or few factors capturing most of the corresponding variance for each case. The resulting individual factor scores were saved for further analyses. We compared these SE modulation factor scores between patients and controls using *t* tests. Nodal SE values were compared between patients and controls in previous reports (Bachiller et al., 2014; Molina et al., 2017a) and therefore not shown here.

Then, after testing for normality and homoscedasticity in the distribution of graph parameters, we applied two stepwise multivariate regression models to assess: (i) the baseline predictors of entropy modulation, and (ii) the correlates of entropy modulation. In both cases, the dependent variables were the SE modulation factor scores. For all the analyses, the level of significance was set to 0.05.

In the first analysis, we introduced the pre-stimulus graph parameters with significant between-group differences as independent (predictive) variables. For the second analysis, independent variables were modulation values in these parameters, showing significant differences between patients and controls. These analyses were separately performed in patients and controls, since previous analyses showed a statistically significant difference between groups for both entropy and graph-parameters (Bachiller et al., 2014; Molina et al., 2017a; Gomez-Pilar et al., 2017) and we hypothesized different associations in both groups. We discarded relevant collinearity effects with tolerance values.

When significant between-groups differences were found we repeated the comparisons including only FE patients and controls to discard that differences were merely an effect of chronicity and/or treatment.

In the group with dMRI data, we studied the associations between structural graph parameters and SE modulation. Since the distribution of structural graph parameters differed from normality in the patients, their association with SE modulation was assessed by means of Spearman correlations.

Clinical and cognitive correlates of graph parameters were assessed using multivariate stepwise regression models, where predictive variables were graph parameters with significant differences between groups. We also calculated the possible relationships between treatment doses, illness duration and functional parameters.

A database with the main data supporting the present results is available (Mendeley Data doi:10.17632/g9crh5b6bz.2).

4. Results

There were no significant differences in age or sex distribution between patients and controls. Patients showed a significant generalized cognitive deficit and reduced P300 amplitude (table 1).

Factor analysis for SE modulation yielded a two-factor solution factor (Table 2) that explained 67.11 % of total variance. The first factor was positively contributed by frontal anterior and medial (Fp1, Fp2, F3, F4, Fz), central (C3, C4, Cz) temporal (T5, T6), occipital (O1, O2), sensors (eigenvalue 10.10, 59.44% of variance), while the second factor was contributed by frontal lateral (F7, F8) and parietal (P3, P4, Pz) sensors (eigenvalue 1.41, 8.33% of variance). Scores for the first factor were significantly higher for the patients ($t = 4.20$, $df = 133$, $p < 0.001$), reflecting a smaller modulation at the sensors included in this factor (since SE values decreased at the response window and thus the difference should be negative). FE patients alone also showed more positive values for the first factor (i.e., smaller SE modulation) than controls (mean 0.206, sd 0.695, $t = 2.03$, $df = 108$, $p = 0.04$)

4.1. Comparison of functional network parameters

Patients showed larger connectivity strength values at the pre-stimulus window (EEG-CS_{PRE}) for the theta band ($t = 3.03$, $df = 133$, $p = 0.003$), and smaller modulation values: *EEG_CLC*$_{MOD}$ ($t = -2.42$, $df = 133$, $p = 0.017$), *EEG-PL*$_{MOD}$ ($t = -2.77$, $df = 133$, $p = 0.006$) and *EEG-CS*$_{MOD}$ ($t = -2.89$, $df = 133$, $p = 0.004$) in that band (Table 3). Those values were used as predictors in further analyses. Chronic patients showed significantly larger EEG-CSPRE values than FE patients, but not significant differences for EEG_CLC_{MOD}, EEG-PL_{MOD} and EEG-CS_{MOD} were found between chronic and FE patients (Table S1, see Supplementary material).

Table 2
Factor structure resulting from the principal components analysis of SE modulation values for each sensor. Factor loads are shown.

	Component	
	1	2
FP1	**0.604**	0.551
FP2	**0.602**	0.527
F3	**0.841**	0.276
F4	**0.739**	0.345
C3	**0.576**	0.492
C4	**0.542**	0.529
P3	0.282	**0.853**
P4	0.267	**0.764**
O1	**0.720**	0.375
O2	**0.704**	0.372
F7	0.377	**0.705**
F8	0.324	**0.751**
T5	**0.666**	0.420
T6	**0.629**	0.378
Fz	**0.918**	0.098
Cz	**0.715**	0.374
Pz	0.268	**0.844**

4.2. Prediction of SE modulation

4.2.1. Functional predictors

In controls, pre-stimulus graph parameters were not predictive of factor scores summarizing SE modulation. In patients, theta band EEG-CS_{PRE} directly predicted scores of the first factor for SE modulation ($R^2 = 0.188$, $df = 1,46$; $F = 10.65$; $\beta = 0.43$; $p = 0.01$; Fig. 2). Thus, a larger average strength of pre-stimulus functional connections in this band was associated with smaller SE modulation (since SE decreased from pre-stimulus to response).

In the FE patients considered alone, pre-stimulus EEG-CS_{PRE} did not predict SE modulation.

4.2.2. Structural predictors

In controls, no significant associations were found between structural brain network parameters and SE modulation ($-0.10 < R < 0.20$). In patients, first factor scores for SE modulation were negatively associated to structural dMRI-CLC ($R^2 = 0.144$, $p = 0.03$). Thus, larger structural clustering was associated to better task-related SE modulation (Fig. 3).

Table 3
Spectral entropy (factor scores) and graph parameters (pre-stimulus and modulation) in patients and controls. Statistically significant differences are marked using asterisks: $^{*}p < 0.05$; $^{**}p < 0.01$; $^{***}p < 0.005$.

	Controls	*Patients*
Entropy modulation factor scores (Factor 1)***	-0.31 (1.13)	0.44 (0.66)
Entropy modulation factor scores (Factor 2)	0.06 (1.12)	-0.13 (0.53)
EEG-CLC$_{PRE}$	1.01 (0.00)	1.01 (0.01)
EEG-PL$_{PRE}$	1.10 (0.02)	1.10 (0.03)
EEG-CS$_{PRE}$**	0.34 (0.04)	0.36 (0.04)
EEG-CLC$_{MOD}$*	0.00 (0.01)	0.00 (0.01)
EEG-PL$_{MOD}$**	0.01 (0.02)	0.00 (0.02)
EEG-CS$_{MOD}$***	0.02 (0.03)	0.01 (0.02)

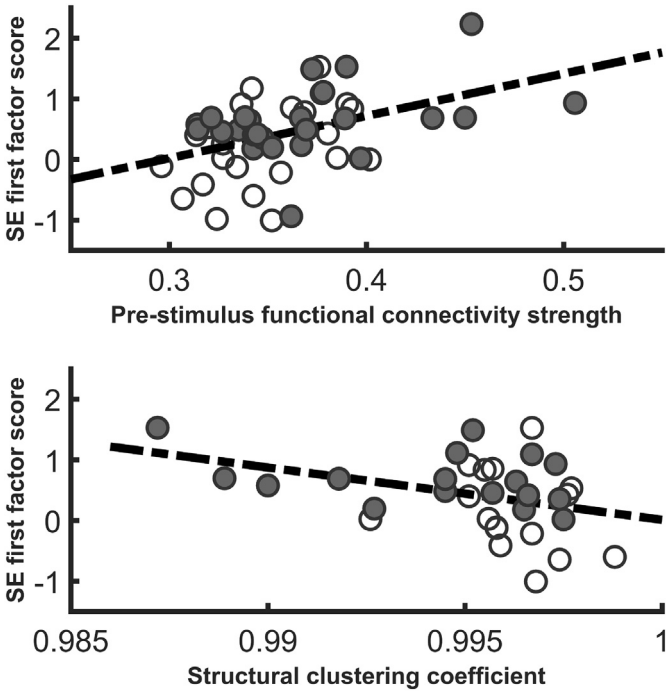

Fig. 2. Scatterplot showing the association in the patients between A) pre-stimulus theta density and SE modulation for the sensors included in the first factor from the principal components analysis and B) between structural clustering coefficient and SE modulation (first factor).

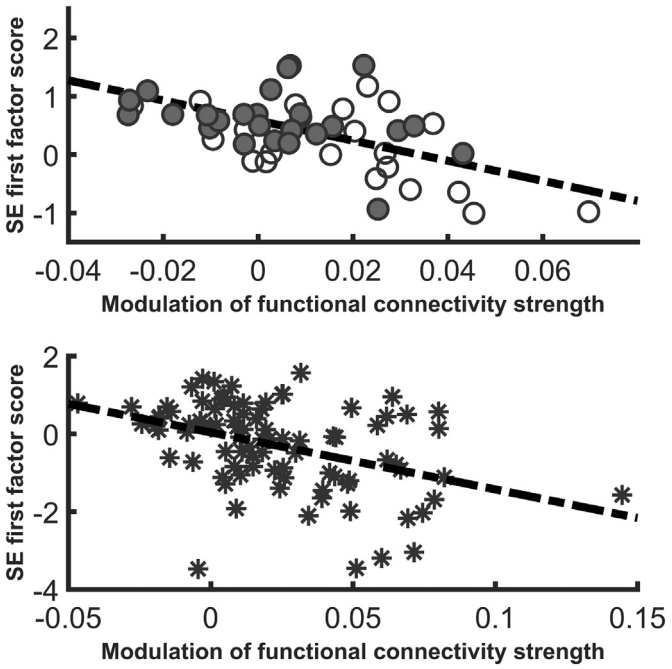

Fig. 3. Scatterplot showing the association of theta band density modulation and SE modulation (first factor) in patients (A) and controls (B). Open circles: FE patients; solid circles: chronic patients; stars: healthy controls). In both groups, the modulation of connectivity strength was inversely associated with SE modulation, but pre-stimulus connectivity strength was associated with SE modulation only for patients (see text).

4.3. Underpinnings of entropy modulation

In controls, first factor scores for SE modulation were inversely associated to *EEG-CS$_{MOD}$* ($R^2 = 0.171$, $df = 1,85$; $F = 17.58$; $\beta = -0.414$, $p < 0.0001$; Fig. 3). Therefore, larger increases of *EEG-CS$_{MOD}$* (i.e., larger global connectivity increases in the theta band from pre-stimulus to response) were associated with more negative values of SE modulation. In other words, larger increases of theta connectivity strength were associated to a higher task related SE modulation, since an SE decrease from pre-stimulus to response is the expected task-related response. SE modulation scores for the sensors included in the second factor were not predicted by network modulation properties in controls.

In patients, SE modulation for the electrodes included in the first factor was similarly inversely associated to *EEG-CS$_{MOD}$* in the theta band ($R^2 = 0.380$, $df = 1,46$; $F = 28.21$; $\beta = -0.617$ $p < 0.0001$; Fig. 3). Therefore, larger increases of theta band *EEG-CS$_{MOD}$* were also associated with higher SE modulation in patients.

In the FE patients considered alone, SE modulation for the first factor was also inversely associated to theta band *EEG-CS$_{MOD}$* ($R^2 = 0.318$, $df = 1,21$; $F = 9.32$; $\beta = -0.564$; $p = 0.006$; Fig. 3).

As in controls, SE modulation scores for the sensors included in the second factor were not predicted by network modulation properties.

4.4. Clinical and cognitive correlates

In the patients, *EEG-CS$_{MOD}$* was inversely associated with negative symptoms ($R^2 = 0.117$, $df = 1,46$; $F = 5.58$; $\beta = -0.343$ $p = 0.023$). In this group, *EEG-CLC$_{MOD}$* predicted verbal memory ($R^2 = 0.102$, $df = 1,46$; $F = 4.54$; $\beta = 0.319$, $p = 0.039$), working memory ($R^2 = 0.208$, $df = 1,46$; $F = 10.25$; $\beta = 0.456$ $p = 0.003$) and verbal fluency ($R^2 = 0.121$, $df = 1,46$; $F = 4.85$; $\beta = 0.348$, $p = 0.035$) performance, and *EEG-PL$_{MOD}$* predicted problem solving performance ($R^2 = 0.190$, $df = 1,46$; $F = 8.92$; $\beta = 0.507$ $p = 0.005$).

In controls, modulation of theta network properties was unrelated to cognitive performance.

There were no significant associations between treatment doses or duration and, on the other hand, SE modulation and network parameters.

5. Discussion

In this study, SE modulation at frontal anterior, central, temporal and occipital electrodes (contributing to most of SE variance) was inversely associated with the pre-stimulus functional connectivity strength (*EEG-CS$_{PRE}$*) in patients. Moreover, a larger theta *CS* increase from pre-stimulus to response windows (*EEG-CS$_{MOD}$*) leads to higher SE modulation.

Our data also reveal a large pre-stimulus theta *EEG-CS$_{PRE}$* in patients. This result, considered together with the smaller change of theta *EEG-CS* modulation (i.e., in the patients, this parameter increased from pre-stimulus to response windows to a smaller degree than in controls), suggests that a hyperactive baseline contributes to a smaller capacity for modulation.

It worth mentioning that the first factor in the PCA included the sensors where significant entropy modulation differences were found in our previous SE comparison between patients and controls (F3, C3, C4, Fz and Cz) (Molina et al., 2017a). Thus, the first factor summarized the modulation in the sensors with significant between-group differences. This would imply that theta *EEG-CS* (both at baseline and its task-related modulation) is relevant to explain the modulation deficits found in schizophrenia.

Connectivity strength represents an average of the graph functional connections. The direct association in the patients between *EEG-CS$_{PRE}$* and SE modulation suggests that a larger number of global functional connections in the pre-stimulus period (in the theta band of the functional network) is associated with a smaller task-related change in SE. This seems coherent with a previous finding at the sensor-lever: larger values of noise power (likely reflecting induced activity) were associated to smaller entropy modulation in a different sample (Molina et al., 2016). Larger broadband (Winterer et al., 2004) and gamma (Diez et al., 2013) noise power was earlier reported in schizophrenia. Taken together, these results support a functional hyper-connectivity

state in schizophrenia patients that may hamper modulation in the functional network, which also seems coherent with previous data with functional magnetic resonance (Manoach, 2003).

Our functional network analysis is based on connectivity derived from PLV between sensors. Since phase synchrony likely reflects the coordinated activation of neural ensembles between regions (Roach and Mathalon, 2008), the larger density values at baseline in the patients might reflect an over-activation of neural ensembles, which, according to their inverse association with SE modulation, hampers the flexibility of neural assemblies with task demands. One possible reason behind these findings might be related to the described inhibitory hypofunction of the cortex in schizophrenia (Lewis et al., 2012), given the role of GABA cells in the appropriate building of transitory neural assemblies underlying cognition (Buzsáki, 2006). Values of $EEG\text{-}CS_{MOD}$ were associated to entropy modulation in both control and schizophrenia groups, whereas in the case of patients, *EEG-CS* was higher at pre-stimulus and its pre-post stimulus modulation was smaller. Therefore, a quantitative difference seems more likely than a qualitative, categorical difference in the underpinnings of such modulation between patients and controls.

It is interesting that negative symptoms were predicted by $EEG\text{-}CS_{MOD}$, but cognitive performance was instead predicted by modulation in $EEG\text{-}CLC_{MOD}$ and $EEG\text{-}PL_{MOD}$. This may imply that cognitive abilities are underpinned by a reorganization of network properties more readily reflected in graph parameters. For instance, local and inter-regional changes in connectivity may be more easily captured by CLC than by SE modulation, even if the latter was previously reduced to two factors and thus likely reflects a more global effect.

The association found in the patients between SE modulation and structural network properties (*dMRI-CLC*) suggests that density and integrity of short-distance structural connections (clustering reflects the connections among regions connected to a given node) facilitates the modulation of functional connectivity. Structural properties (FA) of interregional connections may thus facilitate the formation of neural assemblies underlying task response. Widespread alterations of white matter integrity (which likely produce structural connectivity deficits) have been reported in schizophrenia using dMRI (Ellison-Wright and Bullmore, 2009).

Our work has limitations, most notably the absence of a treatment-naïve group. However, FE patients showed similar patterns of functional connectivity differences and treatment doses did not relate to entropy or graph parameters. Also, since both entropy and density modulation were obtained from the same dataset, it might be considered that their relation would result from data redundancy. However, both parameters reflect completely different properties of EEG dynamics and connectivity strength measurements help characterizing SE deficit in the patients. In addition, EEG is not completely free of volume conduction, even using a reference average approach as in the present study. Nevertheless, dMRI data can be used as control for the field spread effect. Finally, the number of EEG sensors was low, but this may be a relatively minor problem since we did not attempt to localize sources.

In conclusion, our findings suggest that an excess of pre-stimulus functional connectivity in the theta band and a deficit of structural clustering hamper SE modulation of the EEG, and this deficit might be underpinned by a smaller reorganization of connectivity, with a reduced formation of transitory functional connections.

Supplementary data to this article can be found online at https://doi.org/10.1016/j.nicl.2018.02.005.

Acknowledgements

This research project was supported in part by grants from Instituto de Salud Carlos III under project PI15/00299, Consejería de Educacion de Castilla y Leon project VA057P17, “Gerencia Regional de Salud de Castilla y León” under projects GRS 1263/A/16 and GRS 1485/A/17, and “Ministerio de Economía y Competitividad” and FEDER under grants TEC2014-53196-R and TEC2013-44194-P; by ‘European Commission’ and FEDER under project 'Análisis y correlación entre el genoma completo y la actividad cerebral para la ayuda en el diagnóstico de la enfermedad de Alzheimer' ('Cooperation Programme Interreg V-A Spain-Portugal POCTEP 2014-2020'). J. Gomez-Pilar was in receipt of a grant from University of Valladolid and A. Lubeiro was in receipt of a grant from Consejería de Educación de la Junta de Castilla y León.

Role of funding sources

The funding sources had no role in the study design; collection, analysis or interpretation of data; in the writing of the report or the decision to submit the manuscript for publication.

Declaration of interests

The authors have no conflicts of interest to declare.

References

Bachiller, A., Diez, A., Suazo, V., Dominguez, C., Ayuso, M., Hornero, R., et al., 2014. Decreased spectral entropy modulation in patients with schizophrenia during a P300 task. Eur Arch Psychiatry Clin Neurosci. 264 (6), 533–543 (Sep, PubMed PMID: 24496581. Epub 2014/02/06. eng).

Bachiller, A., Poza, J., Gomez, C., Molina, V., Suazo, V., Hornero, R., 2015a. A comparative study of event-related coupling patterns during an auditory oddball task in schizophrenia. J Neural Eng. 12 (1), 016007 (Feb, PubMed PMID: 25474418. Epub 2014/12/05. eng).

Bachiller, A., Romero, S., Molina, V., Alonso, J.F., Mananas, M.A., Poza, J., et al., 2015b. Auditory P3a and P3b neural generators in schizophrenia: an adaptive sLORETA P300 localization approach. Schizophr Res. 169 (1-3), 318–325 (Dec, PubMed PMID: 26481687. Epub 2015/10/21. eng).

Bledowski, C., Prvulovic, D., Hoechstetter, K., Scherg, M., Wibral, M., Goebel, R., et al., 2004. Localizing P300 generators in visual target and distractor processing: a combined event-related potential and functional magnetic resonance imaging study. J Neurosci. 24 (42), 9353-60 (Oct 20, PubMed PMID: 15496671. eng).

Bob, P., Palus, M., Susta, M., Glaslova, K., 2008. EEG phase synchronization in patients with paranoid schizophrenia. Neurosci Lett. 447 (1), 73–77 (Dec 05, PubMed PMID: 18835328. Epub 2008/10/07. eng).

Bressler, S.L., Tognoli, E., 2006. Operational principles of neurocognitive networks. Int J Psychophysiol. 60 (2), 139–148 (May, PubMed PMID: 16490271. Epub 2006/02/24. eng).

Buzsáki, G., 2006. Diversity of Cortical Functions: Inhibition. Rythms of the Brain. Oxford University Press, New York, pp. 61–79.

Dehaene, S., Changeux, J.P., 2011. Experimental and theoretical approaches to conscious processing. Neuron. 70 (2), 200–227 (Apr 28, PubMed PMID: 21521609. Epub 2011/04/28. eng).

Desikan, R.S., Segonne, F., Fischl, B., Quinn, B.T., Dickerson, B.C., Blacker, D., et al., 2006. An automated labeling system for subdividing the human cerebral cortex on MRI scans into gyral based regions of interest. Neuroimage. 31 (3), 968–980 (Jul 01, PubMed PMID: 16530430. Epub 2006/03/15. eng).

Dhollaner T, Connelly A. Unsupervised 3-tissue response function estimation from single-shell or multi-shell diffusion mr data without a co-registered t1 image. ISMRM Workshop on Breaking the Barriers of Diffusion MRI2016.

Di Biase, M.A., Cropley, V.L., Baune, B.T., Olver, J., Amminger, G.P., Phassouliotis, C., et al., 2017. White matter connectivity disruptions in early and chronic schizophrenia. Psychol Med. 22, 1–14 (May, PubMed PMID: 28528586. Epub 2017/05/23. eng).

van Diessen, E., Numan, T., van Dellen, E., van der Kooi, A.W., Boersma, M., Hofman, D., et al., 2015. Opportunities and methodological challenges in EEG and MEG resting state functional brain network research. Clin. Neurophysiol. 126, 1468–1481.

Diez, A., Suazo, V., Casado, P., Martin-Loeches, M., Molina, V., 2013. Spatial distribution and cognitive correlates of gamma noise power in schizophrenia. Psychol Med. 43 (6), 1175–1186 (Sep 11, PubMed PMID: 22963867. Epub 2012/09/12. Eng).

Duff, B.J., Macritchie, K.A., Moorhead, T.W., Lawrie, S.M., Blackwood, D.H., 2013. Human brain imaging studies of DISC1 in schizophrenia, bipolar disorder and depression: a systematic review. Schizophr Res. 147 (1), 1–13 (Jun, PubMed PMID: 23602339. Epub 2013/04/23. eng).

Ellison-Wright, I., Bullmore, E., 2009. Meta-analysis of diffusion tensor imaging studies in schizophrenia. Schizophr Res. 108 (1–3), 3–10 (Mar, PubMed PMID: 19128945. Epub 2009/01/09. eng).

Fischl, B., van der Kouwe, A., Destrieux, C., Halgren, E., Segonne, F., Salat, D.H., et al., 2004. Automatically parcellating the human cerebral cortex. Cereb Cortex. 14 (1), 11–22 (Jan, PubMed PMID: 14654453. Epub 2003/12/05. eng).

Gomez-Pilar, J., Poza, J., Bachiller, A., Gómez, C., Molina, V., Hornero, R., 2015. Neural network reorganization analysis during an auditory oddball task in schizophrenia using wavelet entropy. Entropy. 17, 5241–5256.

Gomez-Pilar, J., Lubeiro, A., Poza, J., Hornero, R., Ayuso, M., Valcarcel, C., et al., 2017. Functional EEG network analysis in schizophrenia: evidence of larger segregation and deficit of modulation. Prog Neuropsychopharmacol Biol Psychiatry. 20 (Mar, PubMed PMID: 28336496. Epub 2017/03/25. eng).

Gomez-Pilar, J., Poza, J., Bachiller, A., Gomez, C., Nuñez, P., Lubeiro, A., et al., 2018. Quantification of graph complexity based on the edge weight distribution balance: application to brain networks. Int. J. Neural Syst. 28 (1), 1750032.

Honey, C.J., Sporns, O., Cammoun, L., Gigandet, X., Thiran, J.P., Meuli, R., et al., 2009. Predicting human resting-state functional connectivity from structural connectivity. Proc Natl Acad Sci U S A. 106 (6), 2035–2040 (Feb 10, PubMed PMID: 19188601. Pubmed Central PMCID: 2634800. Epub 2009/02/04. eng).

Jones, J.T., DiFrancesco, M., Zaal, A.I., Klein-Gitelman, M.S., Gitelman, D., Ying, J., et al., 2015. Childhood-onset lupus with clinical neurocognitive dysfunction shows lower streamline density and pairwise connectivity on diffusion tensor imaging. Lupus. 24 (10), 1081–1086 (Sep, PubMed PMID: 25701565. Pubmed Central PMCID: Pmc4529818. Epub 2015/02/24. eng).

Kay, S.R., Fiszbein, A., Opler, L.A., 1987. The positive and negative syndrome scale (PANSS) for schizophrenia. Schizophr Bull. 13 (2), 261–276 (PubMed PMID: 3616518).

Lachaux, J.P., Rodriguez, E., Martinerie, J., Varela, F.J., 1999. Measuring phase synchrony in brain signals. Hum Brain Mapp. 8 (4), 194–208 (PubMed PMID: 10619414. Epub 2000/01/05. eng).

Lewis, D.A., Curley, A.A., Glausier, J.R., Volk, D.W., 2012. Cortical parvalbumin interneurons and cognitive dysfunction in schizophrenia. Trends Neurosci. 35 (1), 57–67 (Jan, PubMed PMID: 22154068. Pubmed Central PMCID: 3253230. Epub 2011/12/14. eng).

Manoach, D.S., 2003. Prefrontal cortex dysfunction during working memory performance in schizophrenia: reconciling discrepant findings. Schizophr Res. 60 (2-3), 285–298 (Apr 1, PubMed PMID: 12591590).

Mazaheri, A., Picton, T.W., 2005. EEG spectral dynamics during discrimination of auditory and visual targets. Brain Res Cogn Brain Res. 24 (1), 81–96 (Jun, PubMed PMID: 15922161. Epub 2005/06/01. eng).

Molina, V., Bachiller, A., Suazo, V., Lubeiro, A., Poza, J., Hornero, R., 2016. Noise power associated with decreased task-induced variability of brain electrical activity in schizophrenia. Eur Arch Psychiatry Clin Neurosci. 266 (1), 55–61 (Feb, PubMed PMID: 25547316. Epub 2014/12/31. eng).

Molina, V., Bachiller, A., Gomez-Pilar, J., Lubeiro, A., Hornero, R., Cea-Canas, B., et al., 2017a. Deficit of entropy modulation of the EEG in schizophrenia associated to cognitive performance and symptoms. A replication study. Schizophr. Res. http://dx.doi.org/10.1016/j.schres.2017.08.057. (in press, Sep 5. pii: S0920-9964(17)30533-9, Epub ahead of print).

Molina, V., Lubeiro, A., Soto, O., Rodriguez, M., Alvarez, A., Hernandez, R., et al., 2017b. Alterations in prefrontal connectivity in schizophrenia assessed using diffusion magnetic resonance imaging. Prog Neuropsychopharmacol Biol Psychiatry. 76, 107–115 (Mar 10, PubMed PMID: 28288855. Epub 2017/03/16. eng).

Nunez, P., Poza, J., Bachiller, A., Gomez-Pilar, J., Lubeiro, A., Molina, V., et al., 2017. Exploring non-stationarity patterns in schizophrenia: neural reorganization abnormalities in the alpha band. J Neural Eng. 14 (4), 046001 (Aug., PubMed PMID: 28424430. Epub 2017/04/21. eng).

Patenaude, B., Smith, S.M., Kennedy, D.N., Jenkinson, M., 2011. A Bayesian model of shape and appearance for subcortical brain segmentation. Neuroimage. 56 (3), 907–922 (Jun 01, PubMed PMID: 21352927. Pubmed Central PMCID: 3417233. Epub 2011/03/01. eng).

Roach, B.J., Mathalon, D.H., 2008. Event-related EEG time-frequency analysis: an overview of measures and an analysis of early gamma band phase locking in schizophrenia. Schizophr Bull. 34 (5), 907–926 (Sep, PubMed PMID: 18684772. Pubmed Central PMCID: 2632478. Epub 2008/08/08. eng).

Rubinov, M., Sporns, O., 2010. Complex network measures of brain connectivity: uses and interpretations. Neuroimage. 52 (3), 1059–1069 (Sep, PubMed PMID: 19819337. Epub 2009/10/13. eng).

Salvador, R., Pena, A., Menon, D.K., Carpenter, T.A., Pickard, J.D., Bullmore, E.T., 2005. Formal characterization and extension of the linearized diffusion tensor model. Hum Brain Mapp. 24 (2), 144–155 (Feb, PubMed PMID: 15468122. Epub 2004/10/07. eng).

Segarra, N., Bernardo, M., Gutierrez, F., Justicia, A., Fernadez-Egea, E., Allas, M., et al., 2011. Spanish validation of the brief assessment in cognition in schizophrenia (BACS) in patients with schizophrenia and healthy controls. Eur Psychiatry. 26 (2), 69–73 (Mar, PubMed PMID: 20435446. Epub 2010/05/04. eng).

Smith, S.M., 2002. Fast robust automated brain extraction. Hum Brain Mapp. 17 (3), 143–155 (Nov, PubMed PMID: 12391568. Epub 2002/10/23. eng).

Spencer, K.M., Nestor, P.G., Niznikiewicz, M.A., Salisbury, D.F., Shenton, M.E., McCarley, R.W., 2003. Abnormal neural synchrony in schizophrenia. J Neurosci. 23 (19), 7407–7411 (Aug 13, PubMed PMID: 12917376. Pubmed Central PMCID: 2848257. Epub 2003/08/15. eng).

Sporns, O., 2011. Networks for Cognition. Networks of the Brain. MIT Press, Cambridge, Massachussets, pp. 182.

Stam, C.J., de Haan, W., Daffertshofer, A., Jones, B.F., Manshanden, I., van Cappellen van Walsum, A.M., et al., 2009. Graph theoretical analysis of magnetoencephalographic functional connectivity in Alzheimer's disease. Brain. 132 (Pt 1), 213–224 (Jan, PubMed PMID: 18952674. Epub 2008/10/28. eng).

Tanaka, K., 1996. Inferotemporal cortex and object vision. Annu Rev Neurosci. 19, 109–139 (PubMed PMID: 8833438. Epub 1996/01/01. eng).

Tournier, J.D., Calamante, F., Connelly, A., 2007. Robust determination of the fibre orientation distribution in diffusion MRI: non-negativity constrained super-resolved spherical deconvolution. Neuroimage. 35 (4), 1459–1472 (May 01, PubMed PMID: 17379540. Epub 2007/03/24. eng).

Varela, F., Lachaux, J.P., Rodriguez, E., Martinerie, J., 2001. The brainweb: phase synchronization and large-scale integration. Nat Rev Neurosci. 2 (4), 229–239 (Apr, PubMed PMID: 11283746. Epub 2001/04/03. eng).

Winterer, G., Coppola, R., Goldberg, T.E., Egan, M.F., Jones, D.W., Sanchez, C.E., et al., 2004. Prefrontal broadband noise, working memory, and genetic risk for schizophrenia. Am J Psychiatry. 161 (3), 490–500 (Mar, PubMed PMID: 14992975).

Zhang, Y., Brady, M., Smith, S., 2001. Segmentation of brain MR images through a hidden Markov random field model and the expectation-maximization algorithm. IEEE Trans Med Imaging. 20 (1), 45–57 (Jan, PubMed PMID: 11293691. Epub 2001/04/11. eng).